



Nitrite enhanced detection from saliva by simple geometrical modifications of paper-based micromixers

Elham Mollaie¹ · Sasan Asiaei² · Hiwa Aryan^{1,3}

Received: 9 May 2022 / Accepted: 28 September 2022 / Published online: 12 October 2022

© The Author(s), under exclusive licence to Springer-Verlag GmbH Germany, part of Springer Nature 2022

Abstract

Dysregulation of nitric oxide (NO) and its two relatively stable metabolites, nitrite, and nitrate, in SARS-CoV-2, are reported in infected populations, especially for nitrates levels $> 68.4 \mu\text{mol/L}$. In this paper, we measure the abnormal presence of nitrite in the saliva by developing a cheap μPAD for colorimetric detection through the modified Griess reaction. This includes a diazotization reaction between nitrite and Griess reagent, including Sulfanilamide and N-Naphthylethylenediamine in an acidic medium, causing a pink Azo compound. The modifications are suggested by a numerical method model that couples the mass flux with the porosity medium equations (convection, diffusion and, dispersion) that improves the mixing process. The mixing index was quantified from the concentration deviation method via simulation of a homogeneous two-phase flow in a porous environment. Five μPAD designs were fabricated to verify the simulation results of mixing enhancement on the Griess reactants in saliva samples. The investigated geometries include straight, helical, zig-zag, square wave, and inclined jagged shapes fabricated by direct laser writing, suitable for low cost, mass fabrication. Inclined jagged micromixer exhibited the best performance with up to 40% improvement compared with the simple straight geometry. Deliberate geometrical modifications, exemplified here in a jagged micromixer on paper, cut the limit of detection (LOD) by at least half without impacting the linear detection range.

Keywords Nitrite · Saliva · Griess reaction · Microfluidics · Paper-based analytical devices · Point-of-care diagnosis

Abbreviations

BSA	Bovine serum albumin
FEM	Finite element method
LOD	Limit of detection
MUMPS	Multi-frontal massively parallel sparse
NO	Nitric oxide
ODEs	Ordinary differential equations
PARDISO	Parallel direct solver
PDEs	Partial differential equations

POC	Point of care
μPADs	Microfluidic paper-based analytical devices

List of symbols

C [mol/m^3]	Concentration field
D_0 [m^2/s]	Molecular diffusion coefficient
J [$\text{mol}/(\text{m}^2 \text{ s})$]	Total mass flux
M [mol/L]	Molarity
\mathbf{n} [-]	The normal unit vector to boundaries
p [Pa]	Fluid pressure
\mathbf{u} [m/s]	Velocity field vector
S [m]	Dispersivity constant

Greek symbols

η [%]	Mixing efficiency
κ [m^2]	Permeability
μ_G [Pa s]	Griess reagent density
μ_S [Pa s]	Saliva density
ρ_G [kg/m^3]	Griess reagent density
ρ_S [kg/m^3]	Saliva density
Φ [-]	Porosity

✉ Sasan Asiaei
asiaei@iust.ac.ir

¹ School of Mechanical Engineering, Iran University of Science and Technology, Tehran, Iran

² Sensors and Integrated Bio-Microfluidics/MEMS Laboratory, School of Mechanical Engineering, Iran University of Science and Technology, Tehran, Iran

³ Clinical Research Development Center of Imam Khomeini and Mohammad Kermanshahi and Farabi Hospitals, Kermanshah University of Medical Sciences, Kermanshah, Iran

1 Introduction

Microfluidic paper-based analytical devices (μ PADs) have recently drawn considerable attention (Yetisen et al. 2013; Pattanayak et al. 2021), especially for Point-of-Care (POC) applications (Ebrahimi Fana et al. 2021; Tseng et al. 2021; Kishnani et al. 2021) due to their low cost (Mai et al. 2019; Tesfaye and Hussen 2022), wicking transport (Osborn et al. 2010), low volume analysis, multiplexing (Gravesen et al. 1993), user-friendliness (Mehrdel et al. 2018), high efficiency (Wang et al. 2020), and short processing time (Lopez-Ruiz et al. 2014). Owing to their relatively simple and low-cost fabrication equipment (Koivunen et al. 2016), μ PADs have found numerous applications in autonomous technology (Patil et al. 2020), environmental control (Wang et al. 2021b; Damodara et al. 2021), food quality monitoring (Cinti 2019), development of nano-biosensors (Swain and Bhand 2021), and especially detection of various health-related compounds (Eisenbrand et al. 1980; Jayawardane et al. 2014; Sukuroglu et al. 2015; Burleigh et al. 2018; Kamali et al. 2018; Kojić et al. 2020; Ferreira et al. 2021; Shariati and Khayatian 2022), particularly as a rapid, low-cost tool for screening and control of pandemics, such as COVID-19 (Lorente et al. 2020; Verma et al. 2020; Wang et al. 2021a).

Numerous biochemical applications require enhanced micro-mixing of biochemical analytes, which is an intrinsic trait of microfluidic devices, especially μ PADs (Capretto et al. 2011; Zhang et al. 2018a). In μ PADs, due to the porous texture of the paper, capillary forces control the passive mixing of analytes in the device (Rezk et al. 2012; Schaumburg and Berli 2019), which requires to be enhanced to increase the efficiency. As a result, response time is lowered along with the detection limit, exemplified in many applications such as blood sugar testers, protein detection in urine (Gao et al. 2019), or nitrite detectors in serum or saliva (Moorcroft et al. 2001; de Castro et al. 2019). Nitrite and nitrate monitoring require repeated and numerous samplings in patients due to its importance in kidney sophistication, gum infection (Pignatelli et al. 2020) or the blue baby syndrome, gastric cancer (Reed et al. 1981; Jayawardane et al. 2014), the trend of hemodialysis in renal diseases (Klasner et al. 2010), and recently COVID-19 monitoring and screening before and after the infection (Lorente et al. 2020; Wang et al. 2021a). Nitric oxide (NO) metabolites that were identified in the late 1980s (Brizzolari et al. 2021), help as a health status predictor of infected and recovered COVID-19 patients (Lorente et al. 2020; Wang et al.

2021a) due to the Nitrite and Nitrate increased level in blood serum and saliva of COVID-19 patients, especially for non-survivors that leads to cardiovascular dysfunction and bioenergetic failure cellular toxicity (Lorente et al. 2020; Wang et al. 2021a). μ PADs can address this need by enhancing the reactant-biomarker mixing and biochemical reaction (Cardoso et al. 2015).

Nitrite can be measured by various methods such as colorimetry (Zhang et al. 2018b), chromatography (Barciela Alonso and Prego 2000; Jobgen et al. 2007), spectrophotometry (Miranda et al. 2010; Irandoust et al. 2013; Wang et al. 2018) and electrochemistry (Badea et al. 2001). Most of these methods are costly and require an educated operator and sophisticated equipment (Chauhan and Toley 2021), and thus not suitable for mass screening and monitoring.

However, the colorimetric method (Zhang et al. 2018b), especially using Griess reaction (Shinn 1941; Ferreira et al. 2020; Cai et al. 2021) and a cost-effective platform, such as μ PADs is simply conducted with arbitrary detection and a relatively vast linear concentration range. Numerous studies have addressed nitrite detection by the Griess method in μ PADs (Wang et al. 2017; Liu et al. 2018; Dudala et al. 2019; Trofimchuk et al. 2020). Parameters investigated include the effect of temperature on color development, the acidity of the environment and its impact on the color intensity (Bhakta et al. 2014), color stability (Klasner et al. 2010; Bhakta et al. 2014), extruding the μ PAD into 3D (Jayawardane et al. 2014), and reducing the fabrication time (Klasner et al. 2010). Nevertheless, the effect of micromixer geometry on mixing efficiency for nitrite detection and its implications for performance enhancement has not been much dealt with yet. Moreover, the linear range was sacrificed to improve the LOD, which limits the application range. On the other hand, the efficiency of the nitrite analyzer depends on the performance of the passive paper-based micromixer, which is highly dependent on the channel structure design (Gidde and Pawar 2020).

In this paper, The modified Griess reaction (Tsikas 2007) method is selected for detection due to the convenience of visible change in a biological sample upon the presence of nitrite. A paper-based micromixer mixes the sample and runs the Griess reaction. We numerically and experimentally examine the outcomes of simulations and experiments among five different geometries to adapt a suitable one, increase the mixing efficiency, and enhance the detection accuracy. The designed μ PADs were fabricated by a facile and cost-effective laser cutting method. By improving the mixing of the reagent and sample in small dimensions, these μ PADs were illustrated to simultaneously enhance the sensitivity and linear detection range.

2 Materials and methods

2.1 Numerical study

This section introduces the proposed geometry models, the applied boundary conditions, the main equations, and the numerical method used to numerically solve the two-phase mass transport problem and explore its effect on mixing efficiency.

2.1.1 Geometry and boundary conditions

To study the effect of channel structure on the mixing efficiency and select the most practical geometry, five μ PAD designs with two inlets, a mixing channel, a detection zone, and an outlet were examined (Fig. 1). Normal inflow velocity was measured using a digital microscope (Coolingtech, Guangdong, China). 10 μ L of sample was dispensed and the movement of fluid through the porous medium was recorded in real time. At each runway direction, the average flow velocity was measured on the pad for at-least four consecutive equally spaced distances, (Asiaei et al. 2018), and the result was used as a normal inflow velocity of 5 mm/sec as a boundary condition. The boundary conditions applied

Table 1 Boundary conditions at the inlets and outlet

Boundary	Normal inflow velocity	Nitrite concentration	Pressure
Inlet 1	5 mm/s	10 mM	–
Inlet 2	5 mm/s	0	–
Outlet	–	–	0 Pa

to each part of the μ PADs are illustrated in (Table 1). In the design of geometries, the significant factors such as channel width, length of the mixing zone, number of fractures, and output length were kept the same for all the designs; the total height of the mixing zone is 3 mm in all four optimized proposed cases.

2.1.2 Governing equations

In the first step, the dynamics of capillary-driven fluid are resolved to procure a macroscopic velocity field u , clarified by the fluid viscosity, porosity, permeability, and the geometrical boundaries of the fluid zone. Coupled with this velocity field, the macroscopic species concentration field C is utilized as follows (Elizalde et al. 2015):

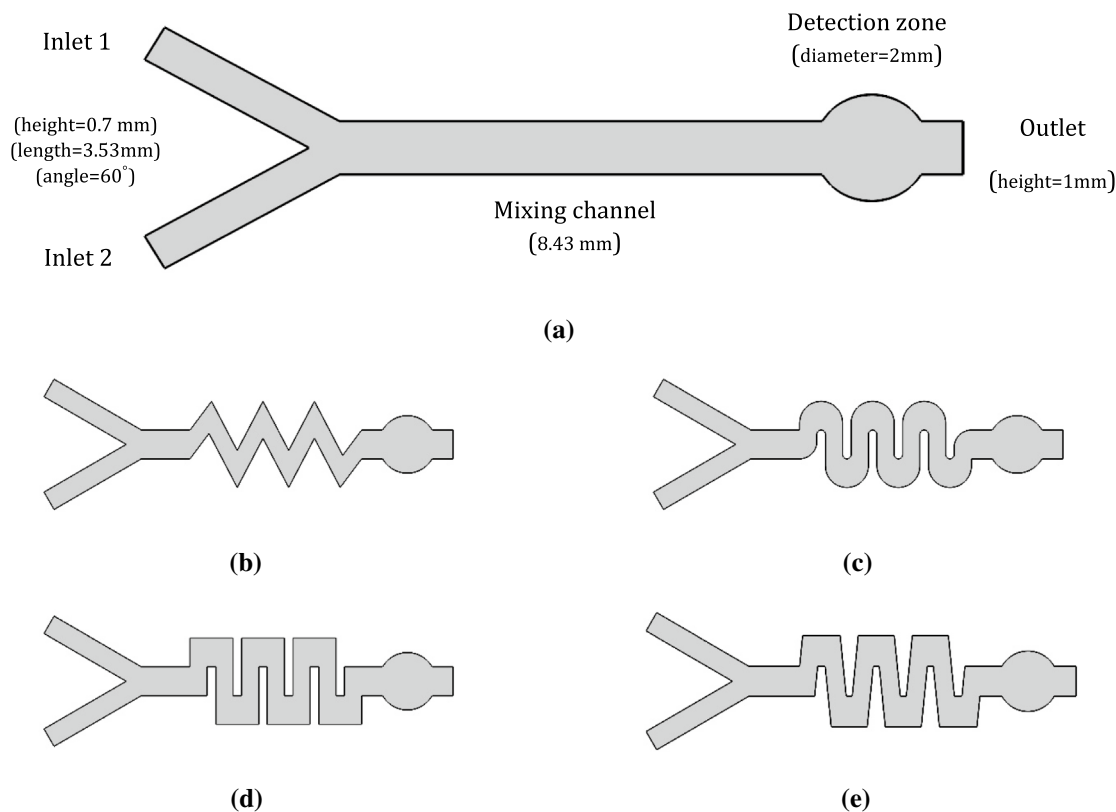


Fig. 1 Five different geometries were used in the numerical simulations, **a** straight, **b** zig-zag, **c** helical, **d** square-wave, and **e** inclined-jagged

$$\frac{\partial C}{\partial t} = \nabla \cdot \mathbf{J}, \tag{1}$$

where J is the species' total mass flux and is derived from the linear superposition of advection, diffusion, and mechanical dispersion transport mechanisms, respectively, by the following equation (Schaumburg et al. 2018; Zaglavara et al. 2022):

$$\mathbf{J} = \mathbf{u}C - D_0 \nabla C - s|\mathbf{u}| \nabla C, \tag{2}$$

where D_0 is molecular diffusion coefficient and s is the dispersivity constant, which demonstrates a characteristic dimension of the porous fiber network microstructure (Urteaga et al. 2018).

The inlet flow is supposed to be pseudo-stationary and free of inertia, concurring with the extremely low local Reynolds numbers. The system is assumed under isothermal conditions and with a controlled humidity level. Gravity is ignored in the studies. With these assumptions, the mass conservation equation for incompressible fluids can be coupled to Darcy's law for each phase, as follows (Hong et al. 2021; Karimi et al. 2021; Hao et al. 2021):

$$\nabla \cdot (\phi \mathbf{u}) = 0, \tag{3}$$

$$\mathbf{u} = -\frac{\kappa}{\mu \phi} \nabla p, \tag{4}$$

where κ is the paper permeability, μ is the fluid viscosity, ϕ is the substrate porosity, and ∇p is the pressure gradient. These expressions can be combined and employed for calculating the pressure field. Then the concentration field is obtained as the following boundary value problem (Schaumburg et al. 2018):

$$\frac{\partial C}{\partial t} = \nabla \cdot (\mathbf{u}C - D_0 \nabla C - s|\mathbf{u}| \nabla C), \tag{5}$$

$$C = C_0 \text{ at saliva inlet,}$$

$$\nabla C \cdot \mathbf{n} = 0 \text{ at outlets and walls,}$$

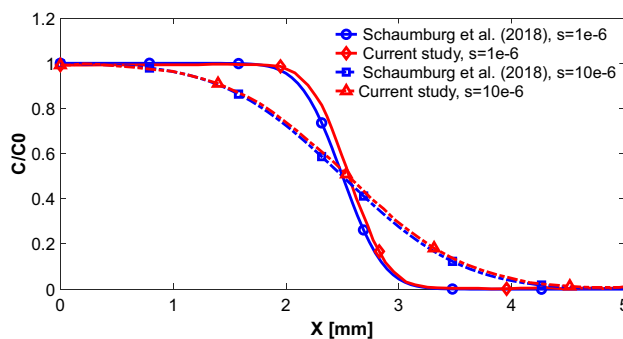


Fig. 2 Relative concentration as a function of transverse distance

where \mathbf{n} is the normal vector to the boundaries. The previously mentioned parameters values used in this work are illustrated in (Table 2) (Noiphung et al. 2018; Schaumburg et al. 2018; Govindaraj et al. 2019).

2.1.3 Numerical method

Numerical simulation is carried out using the finite element method (FEM), approximating the governing partial differential equations (PDEs) with numerical model equations using discretization methods. The mentioned governing equations are coupled together and solved by separate stationary solvers in two study steps provided by COMSOL Multiphysics 5.6. Two different physics are applied and coupled to resolve this problem. Two-phase Darcy's law (tpdl) is used to solve the velocity and pressure fields simultaneously with the discretization of (P2 + P1) for pressure and fluid content, respectively, using a MUMPS (Multi-frontal massively parallel sparse) direct solver to obtain the mentioned fields. Transport of Diluted Species in Porous Media (tds) is utilized to obtain the concentration field with linear discretization and is solved using the PARDISO (Parallel direct solver) solver. Relative tolerances used to satisfy the convergence criteria for the two-mentioned steps are considered as 10^{-3} (Aryan et al. 2022).

Table 2 Parameters value used in the numerical simulations

Parameter	Value
Saliva viscosity	$\mu_s = 0.0014[\text{Pa}\cdot\text{s}]$
Saliva density	$\rho_s = 1000[\text{kg}/\text{m}^3]$
Griess reagent viscosity	$\mu_G = 0.00095[\text{Pa}\cdot\text{s}]$
Griess reagent density	$\rho_G = 981[\text{kg}/\text{m}^3]$
Whatman filter paper No. 1 porosity	$\phi = 0.68$
Whatman filter paper No. 1 permeability	$\kappa = 7.5 \times 10^{(-16)}[\text{m}^2]$
Molecular diffusion coefficient	$D_0 = 6.5 \times 10^{(-10)}[\text{m}^2/\text{s}]$
Whatman filter paper No. 1 dispersivity constant	$S = 1 \times 10^{(-6)} [\text{m}]$

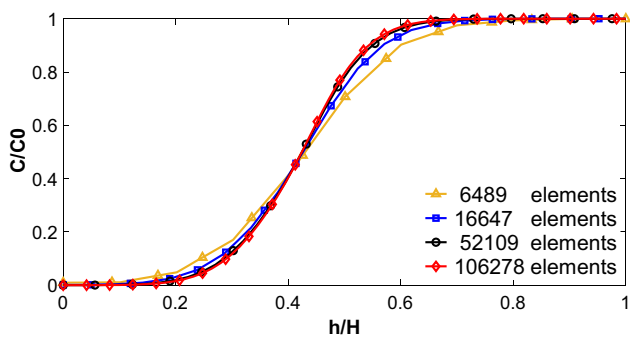


Fig. 3 Comparison of the numerical results with different grids showing relative concentration

2.1.4 Validation

To verify the numerical model, our simulation results are compared with the work of Schaumburg et al. (Schaumburg et al. 2018). In all cases, the numerical model satisfactorily predicts the expected behavior (Fig. 2).

2.1.5 Grid independence

A mesh independence study is performed to reduce the computational cost while achieving accurate grid-independent results. The relative concentration at the middle of the mixing channel of the straight geometry is reported for different grids to check the grid independence. According to the results illustrated in (Fig. 3), the case with 52,109 elements could provide accurate and independent results from the computational grid.

2.2 Experimental study

The experiments include three steps: micromixer preparation, Griess experiment, and image analysis. First, each paper-based micromixer was prepared by laser cutting. Then Griess reaction was conducted, and ultimately the taken images of the detection zone were analyzed by image processing software.

2.2.1 μPAD fabrication

For fabrication of the μPADs, we have examined and used a simple, modified CO2 laser cutting process, also suitable for mass, reliable, and low-cost production (Nie et al. 2012). The angles were considered 85° and 62° for inclined jagged and zig-zag geometries, respectively. The paper used was the No. 1 Whatman® (VWR; Radnor, PA) paper. Whatman 1 paper is used due to its adequate porosity/permeability that entails a proper flow velocity of around 5 mm/s and accordingly enhanced performance for

processing of our saliva samples, such as LOD and linear range. Higher grades, such as Whatman 2, the porosity decreases and the pad is more absorbent, not favorable for our future applications of whole blood or plasma analysis. Moreover, decrease in porosity would decrease the flow velocity and thus the replenishment rate of reactants and lower the overall performance. Grade 1 paper has a higher availability in market, and also in scientific/technical reports (Martinez et al. 2007) compared to higher grades. This made our fabrication, verification (Busa et al. 2016) and correlation steps in Nitrite more straight forward (He et al. 2013; Jayawardane et al. 2014; Lopez-Ruiz et al. 2014; Cardoso et al. 2015). Cutting should be carried out very slowly (cutting rate of 20 mm/s) and at low power (laser power of 40 W) at the applied current of 5 mA. The two inlets with a length of 3.53 mm and a width of 0.7 mm have a 60° angle with each other. All mixers have a fixed

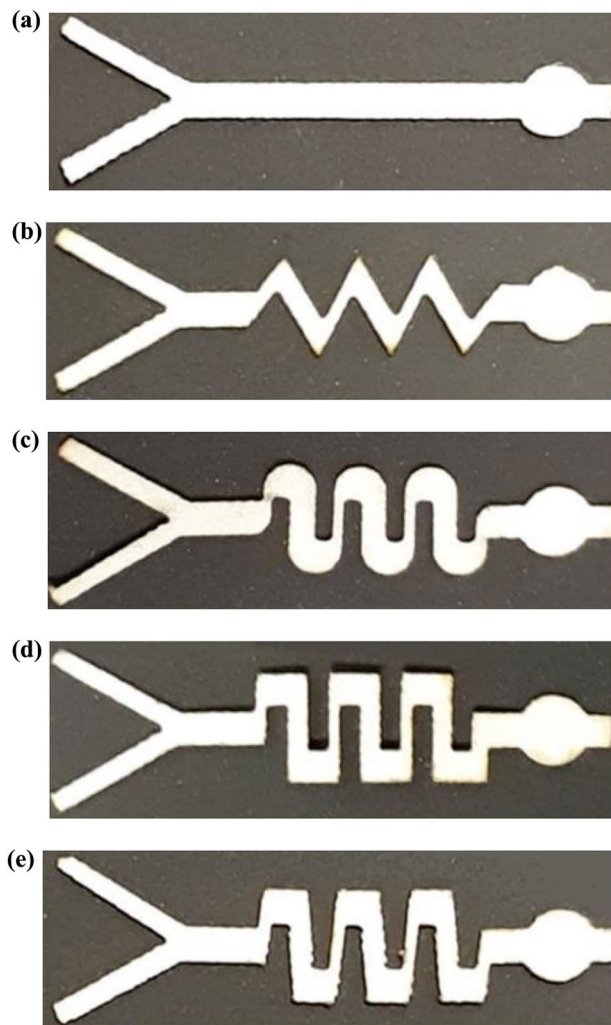


Fig. 4 Five different geometries were fabricated by laser-cut. **a** straight, **b** zig-zag, **c** helical, **d** square-wave, and **e** inclined-jagged, design

width of 1 mm and 8.43 mm in length. The diameter of the detection zone was 2 mm. The total length of the device is the same in all micromixers and is equal to 14.31 mm (Fig. 4).

2.2.2 Griess reaction

Nitrite detection was conducted based on the modified Griess method, which is a diazotization reaction (Tsikas 2007). Nitrite is reacted in an acidic environment by a reagent, i.e., sulfanilamide, which results in a diazonium salt. Next, diazonium salt will be converted to a stable AZO compound by a linking reagent such as N-naphthyl- ethylenediamine, a pink compound (Shinn 1941; Sun et al. 2003). In the modified Griess reaction, using sulfanilamide in an acidic medium like hydrochloric acid instead of sulfanilic acid causes better color stability and faster kinetics (Shinn 1941; Frenzel et al. 2004; Cardoso et al. 2015). First, for preparing the Griess reagent, acid-soluble sulfanilamide 1% (Sigma–Aldrich; St. Louis, MO) and water-soluble N-naphthyl- ethylenediamine dihydrochloride 0.1% (NED; Merck Millipore, Germany) was mixed with equal volumetric ratios (Bhakta et al. 2014). We used hydrochloric acid 10% to create the needed acidic environment. In the next step, artificial saliva was prepared according to (Yıldırım et al. 2003); which included 0.4 mg/ml sodium chloride (Sigma–Aldrich; St. Louis, MO), 0.4 mg/ml potassium chloride (Gibbstown NJ EM Science;), 0.8 mg/ml calcium chloride (Alfa Aesar; Ward Hill, MA), 0.69 mg/ml sodium dihydrogen phosphate (Fisher Scientific; Waltham, MA) and 0.0163 mg/ml sodium sulfide (Sigma–Aldrich; St. Louis, MO) in the base solution of 10 mmol/L sodium nitrate (Merck Millipore, Germany). Before running the experiment, the micromixer was placed in BSA protein solution for 30 min as a preprocessing blocking process (Kamali et al. 2018).

Generally, Griess reagent cannot be stored for more than 8 h (Green et al. 1982). We should keep the Griess reagent in an opaque jar wrapped in aluminum foil and performed the experiments in a dark room (Lopez-Ruiz et al. 2014; Cardoso et al. 2015). With these measures, we could safely use a stable Griess reagent in a maximum of 3.5 h period.

To avoid the stability issues of premixed Griess Reagent, first, we mixed the artificial saliva and Sulfanilamide together and added NED separately, thus Griess constituents are not priory combined (Sun et al. 2003). After drying the paper, We put a 5 μ L drop of NED in the detection zone (Li et al. 2014; Lopez-Ruiz et al. 2014), before placing the sample and sulfanilamide in the 2 inlets. After 10 min a 5 μ L drop of sulfanilamide was placed on inlet 2; then, a drop of saliva with the same volume was placed on inlet 1. Due to the capillary properties, the drops will advance through the channel. After a specific time, the presence of nitrite

in saliva will be confirmed by the emergence of pink color in the detection zone.

2.2.3 Detection technique

The intensity of the color of the Griess reaction in a sample depends on the nitrite ion concentration. Due to the short length of the paper-based device, the volume of the reagent is also low. In the case of nitrite present in the analyzed samples, the sensor responds in a few minutes. The unaided eye can easily observe the created pink color. For quantifying the amount of nitrite, an image was taken from the device after the test, and the analyses of the presence of nitrite were performed by image processing algorithms developed using MATLAB (Choobbari et al. 2020). The color intensity was measured according to the scanned images' RGB color codes (Rhouma et al. 2009; Asiaei et al. 2018). The performance of the five geometries, as mentioned above, is assessed by image colorimetry processing. Each pixel is processed and averaged on the whole circle. A higher pick and minimum deviation from the mean are translated to a satisfactory mixing performance.

In contrast, a low pick and scattered RGB intensity correspond to lower or improper mixing efficiencies. After 7 min from the reaction initialized and, therefore, color stabilization, the detection zone was imaged by a smartphone's camera (GALAXY A6+) (Cardoso et al. 2015). The color intensity gradually increased on the micromixers until it converged to a constant value. For reliability and trend assessment, images were taken from the μ PAD every minute. After this time, the stable images of μ PADs were considered as the criteria for the concentration of nitrite from RGB values. The mean of the RGB of all points of the detection zone was calculated using a home-developed MATLAB image processing code. For more accuracy, all photos were taken at a specific period demonstrated in a day and a fixed location. All the analyses were calibrated by considering an area as a reference in each photo to eliminate the slightest errors. In this way, the effect of light or operating error could be avoided as much as possible. Each data point trial was repeated at least six times and averaged.

3 Results and discussion

We used a mixing section between the input segment and the detection zone, which adds complexity to the geometry and raises the disorders to increase the mixing efficiency and decrease the detection limit. The performance of the corresponding μ PAD was examined for

nitrite detection to confirm the impact of enhanced mixing on the detection performance.

3.1 Effect of inlet angle on mixing efficiency

The impact of the inlet angle between two phases' entry channels on the mixing efficiency was numerically evaluated. For this reason, six different inlet angles were modeled and simulated based on the straight geometry, as shown in (Fig. 5). According to (Fig. 6), the mixing efficiency is not much dependent on the inlet angle (less than 2%) because the two entry flows do not affect each other until the mixing channels' entry, where the stream lines are cut by the boundary geometry lines. The 60 degrees inlet angle is selected rather arbitrary and a minor fact was the easier movement of the laser cutter on mutual 60 degrees from vertical upward to the entry channel (60 degrees rotation) and then from the upper entry to lower entry and then to the downward vertical direction. This angle was then used in both numerical and experimental studies.

3.2 Comparison of μ PADs efficiency

For the concentration fields obtained results are as shown in (Fig. 7), the five studied geometries' mixing efficiencies were determined from the numerical simulations and by the image post-processing of the experimental results. For the analysis, the concentration relative deviation criterion was used as follows (Jain et al. 2013):

$$\eta = \left[1 - 2 * \sqrt{\frac{\int_A (\bar{c} - \bar{c}^*)^2 dA}{\int_A dA}} \right], \tag{6}$$

where the variable \bar{c} shows the scaled concentration value at each point while \bar{c}^* represents the scaled concentration

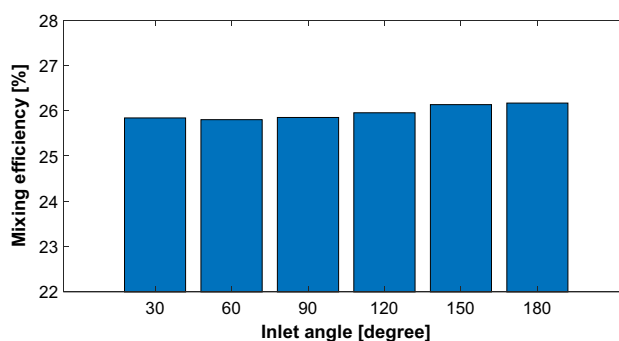


Fig. 6 Mixing efficiency results of the six different studied inlet angles

at each point of a thoroughly mixed solution (i.e., 0.5), and A denotes the area where the mixing criterion is calculated (Jain et al. 2013). Consequently, in each computational cell, the closer the local concentration value is to 0.5, the closer the efficiency value is to one. One hundred percent efficiency means that two substances are found equally in all cells of the studied section. Hence, by adding curvature, the length of the straight model increases; besides the proposed geometries, four more straight geometries with the same path-lines length as the four curvature models are investigated numerically to find good insight into the effect of both length and curvature shape on mixing efficiency, as shown in (Fig. 8).

Adding complexities increases the effective length and the contact time, as well as irregularity (Rezk et al. 2012). Upon proper modeling and design, adding irregularities in the flow path-line also increases the flow resistance in the unit length of the pad, which decreases the flow velocity and allows for better mixing. As the results reveal, mixing efficiency generally increases by adding curvature to the straight micromixer. The inclined-jagged model has

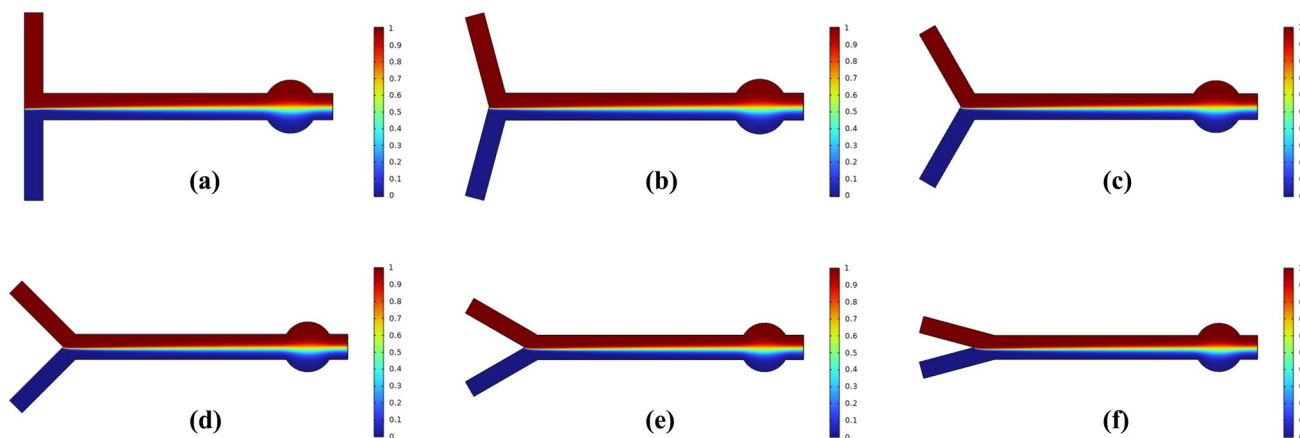


Fig. 5 The concentration field results of Six different inlet angles modeled and simulated, a 180, b 150, c 120, d 90, e 60 and, f 30 degrees

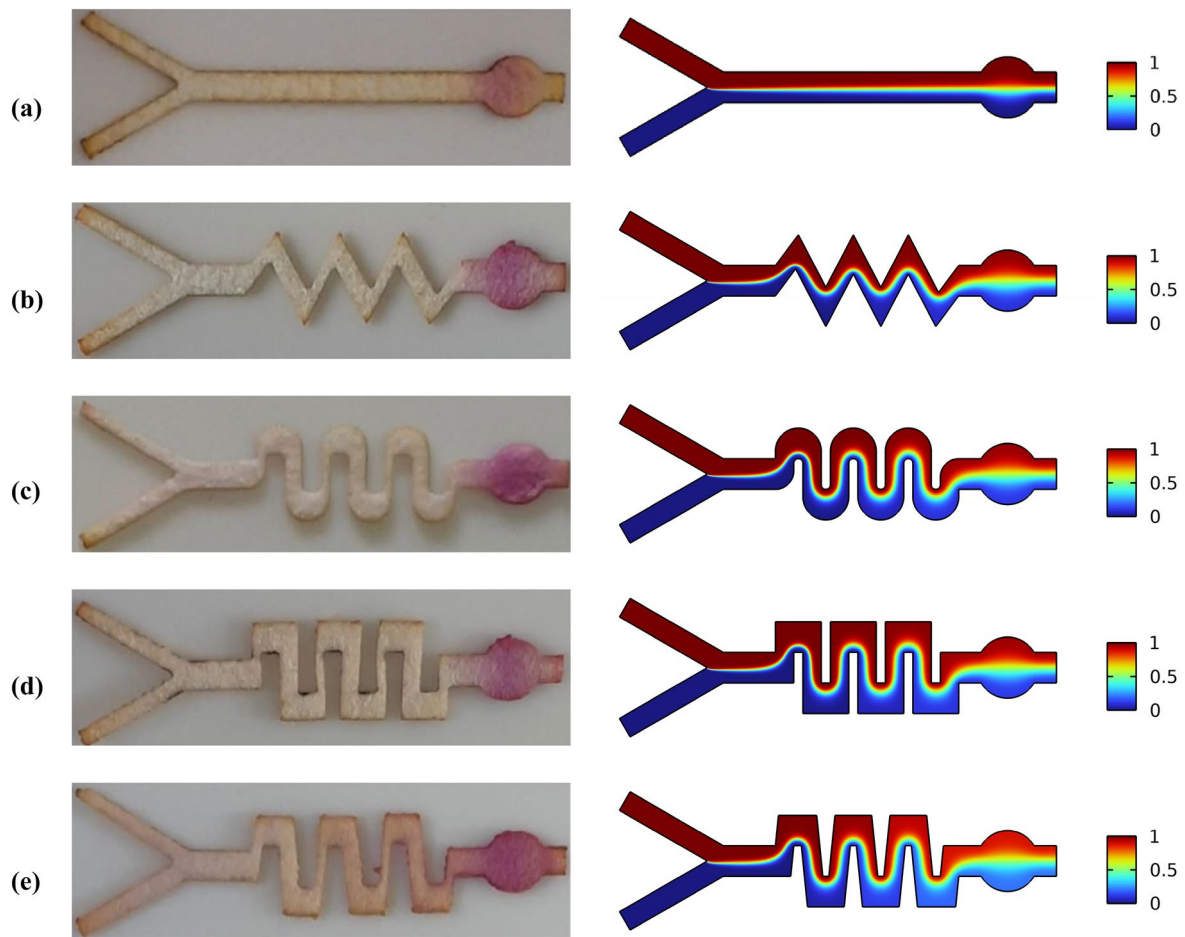
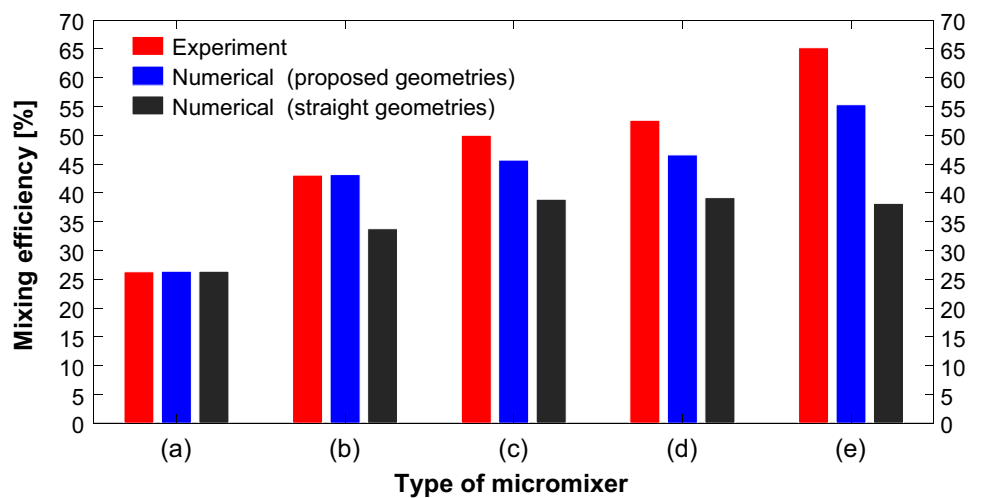


Fig. 7 Numerical and experimental results of nitrite relative concentration field (right side) and nitrite detection test (left side) for **a** straight, **b** zig-zag, **c** helical, **d** square-wave, and **e** inclined-jagged, geometries

Fig. 8 Experimentally and numerically obtained mixing efficiency for **a** straight, **b** zig-zag, **c** helical, **d** square-wave, and **e** inclined-jagged, geometries



the best mixing performance compared with all the other studied geometries. The results showed that for two different paper-based micromixers, one with a straight mixing channel and the other with a curved mixing channel, the one with a curvature has a higher mixing efficiency due to its novel curved geometry.

3.3 Determination of LOD with inclined jagged micromixer

Artificial saliva samples with different nitrite concentrations from zero to 1000 μM were tested by inclined jagged μPAD to determine the limit of detection (LOD) and measurement range.

Other geometries did not result in conclusive, reliable/repeatable detection results for analyte concentrations below 10 μM , presumably due to inferior mixing quality and/or local trapping/concentration of analytes.

To determine the LOD, analyte concentrations of 0, 5, 5.5, 5.6, 5.7, 14.2, 25.6, 57.1, 114.3, 500 and 1000 μM were serially examined. Each data point was recorded after repeating for 10 times for each pad configuration and concentration, reading different pads. The color intensity was evaluated after stabilization in 7 min from the start time of the test and recorded with a statistical significance cut-off of 0.05. Concentrations between 0 and 5.6 μM did not yield reliable results; not only the color change was not visually conclusive (minor or incomplete color changes), but also the color intensity was less than 3 times of the

noise in baseline (Shrivastava and Gupta 2011). Artificial saliva was prepared, nitrite concentration was gradually increased from zero to 1000 μM , and the test was repeated each time. The detection zone showed no color variation until the concentration of 5.7 μM , as shown in (Fig. 9). To propose the outcomes of the test as a database, the final results and the curve fitting plot is illustrated in (Fig. 10a). The reports have become linear and are shown in (Fig. 10b) to make this more user-friendly.

The demonstrated LOD and linear range enables drawing meaningful conclusions for COVID-19 and other Nitrite/nitrate marked disease. Compared to healthy subjects, higher nitrate and nitrite levels were observed in COVID-19 patients (Lorente et al. 2020), around 20 μM . Nevertheless, the levels were not significantly different among mild-, common-, severe and critical-type patients who recovered from COVID-19 disease (Lorente et al. 2020; Wang et al. 2021a). On the other hand, for non-survivors, higher nitrate and nitrite levels have been shown about 86 μM , which could be due to a higher nitric oxide production (Lorente et al. 2020).

3.4 Performance analysis of inclined jagged micromixer with natural saliva samples

We used our μPAD on several accurate saliva samples from at least five volunteers between 25 and 42 years for each data point to validate nitrite detection in the inclined jagged micromixer against an HPLC–UV method apart from

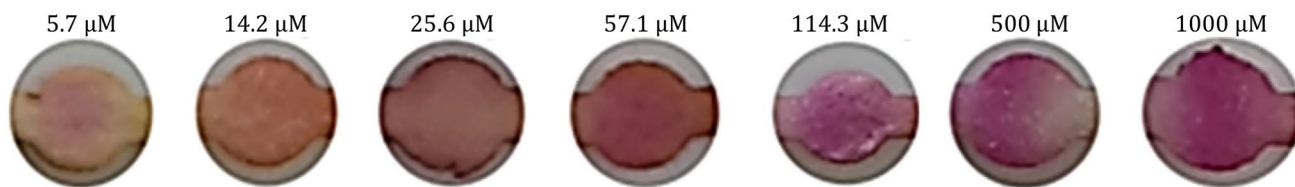


Fig. 9 Detection of nitrite in artificial saliva with different concentration ranges

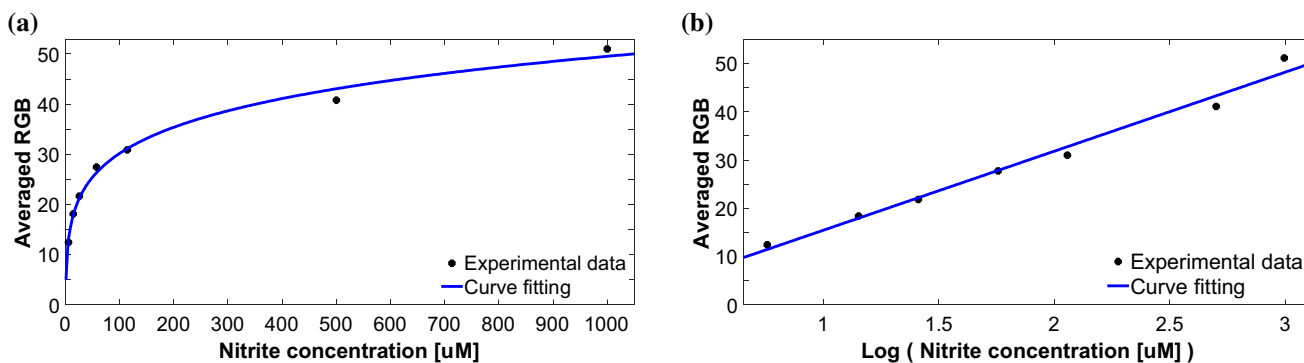


Fig. 10 Detection of nitrite concentration by Averaged-RGB value a linear-scale, b logarithm-scale

Table 3 Comparison of the nitrite detection result from inclined jagged micromixer and UV-based method

Volunteers	Jagged inclined micromixer (nitrite) [μM]	HPLC–UV (nitrite) [μM]	Error (%)
#1	33 \pm 2	33.9 \pm 0.2	5.6
#2	193 \pm 15	182.8 \pm 0.2	5.6
#3	126 \pm 9	121.1 \pm 0.2	4
#4	27 \pm 2	28.2 \pm 0.2	4.2
#5	44 \pm 3	42.5 \pm 0.2	3.5

their health status. (Table 3) shows the measurement results and their comparison with the HPLC–UV method (Agilent Infinity Series 1260–DAD). As demonstrated, nitrite samples were in the range of 27 μM to 193 μM , and all the tests were confirmed with less than 5% of deviation from the clinical method for all candidates.

4 Conclusions

In this paper, nitrite detection was conducted on paper-based micro-devices by the colorimetric method. To reach better performances, the μPADs were first numerically modeled and simulated to find the model with the optimized geometric mixing efficiency, and their efficiency at the next step was examined and verified experimentally. Deliberate geometric irregularities improve the mixing efficiency of nitrite content of saliva by almost 70%, resulting in enhanced color signals for nitrite content quantification. Modification of μPADs geometries showed that the inclined jagged shape cuts the detection limit to 5.7 μM without sacrificing the detection range from 5 to 1000 μM . This method can be in a low resourceful setting due to ease of fabrication (laser cutting) and relatively low cost of chemicals.

Moreover, due to the microscopic dimensions of the micromixer, the reaction time is concise, about 25 s. We should only give it 7 min for drying and color stabilization; thus, the overall process time and cost are much less than conventional methods. Regarding the extensive application of the mixing in passive paper-based microfluidic applications, the presented mixing enhancement methodology can be employed for several reactions and detection of other compounds.

Acknowledgements The authors would also like to acknowledge the products and services provided by Prof. Mohammad Javad Rasaei, Dr. Babak Kamali, and Ali Zadeh Kafi that facilitated this research.

Funding This work has received no funding.

Declarations

Conflict of interest The authors declare that they have no conflict of interest.

References

- Aryan H, Beigzadeh B, Siavashi M (2022) Euler-Lagrange numerical simulation of improved magnetic drug delivery in a three-dimensional CT-based carotid artery bifurcation. *Comput Methods Programs Biomed* 219:106778. <https://doi.org/10.1016/j.cmpb.2022.106778>
- Asiaei S, Bidgoli MR, ZadehKafi A et al (2018) Sensitivity and colour intensity enhancement in lateral flow immunoassay tests by adjustment of test line position. *Clin Chim Acta* 487:210–215. <https://doi.org/10.1016/j.cca.2018.10.001>
- Badea M, Amine A, Palleschi G et al (2001) New electrochemical sensors for detection of nitrites and nitrates. *J Electroanal Chem* 509:66–72. [https://doi.org/10.1016/S0022-0728\(01\)00358-8](https://doi.org/10.1016/S0022-0728(01)00358-8)
- Barciela Alonso MC, Prego R (2000) Determination of silicate, simultaneously with other nutrients (nitrite, nitrate and phosphate), in river waters by capillary electrophoresis. *Anal Chim Acta* 416:21–27. [https://doi.org/10.1016/s0003-2670\(00\)00865-5](https://doi.org/10.1016/s0003-2670(00)00865-5)
- Bhakta SA, Borba R, Taba M et al (2014) Determination of nitrite in saliva using microfluidic paper-based analytical devices. *Anal Chim Acta* 809:117–122. <https://doi.org/10.1016/j.aca.2013.11.044>
- Brizzolari A, Dei Cas M, Cialoni D et al (2021) High-throughput Griess assay of nitrite and nitrate in plasma and red blood cells for human physiology studies under extreme conditions. *Molecules* 26:4569. <https://doi.org/10.3390/molecules26154569>
- Burleigh MC, Liddle L, Monaghan C et al (2018) Salivary nitrite production is elevated in individuals with a higher abundance of oral nitrate-reducing bacteria. *Free Radical Biol Med* 120:80–88. <https://doi.org/10.1016/j.freeradbiomed.2018.03.023>
- Busa LSA, Mohammadi S, Maeki M et al (2016) Advances in microfluidic paper-based analytical devices for food and water analysis. *Micromachines (Basel)* 7:86. <https://doi.org/10.3390/mi7050086>
- Cai R, Lu D, She Q et al (2021) Reusable 3D silver superposed silica SERS substrate based on the Griess reaction for the ratiometric detection of nitrite. *Anal Bioanal Chem* 413:4751–4761. <https://doi.org/10.1007/s00216-021-03429-x>
- Capretto L, Cheng W, Hill M, Zhang X (2011) Micromixing within microfluidic devices. *Top Curr Chem* 304:27–68. https://doi.org/10.1007/128_2011_150
- Cardoso TMG, Garcia PT, Coltro WKT (2015) Colorimetric determination of nitrite in clinical, food and environmental samples using microfluidic devices stamped in paper platforms. *Anal Methods* 7:7311–7317. <https://doi.org/10.1039/C5AY00466G>
- Chauhan A, Toley BJ (2021) Barrier-free microfluidic paper analytical devices for multiplex colorimetric detection of analytes. *Anal Chem* 93:8954–8961. <https://doi.org/10.1021/acs.analchem.1c01477>
- Choobbari ML, Rad MB, Jahanshahi A, Ghourchian H (2020) A sample volume independent paper microfluidic device for quantifying glucose in real human plasma. *Microfluid Nanofluid* 24:74. <https://doi.org/10.1007/s10404-020-02382-y>

- Cinti S (2019) Novel paper-based electroanalytical tools for food surveillance. *Anal Bioanal Chem* 411:4303–4311. <https://doi.org/10.1007/s00216-019-01640-5>
- Damodara S, Zhu Y, Selvaganapathy PR (2021) Patterned threads as solid-state reagent storage and delivery medium for automated periodic colorimetric monitoring of the environment. *Microfluid Nanofluid* 25:93. <https://doi.org/10.1007/s10404-021-02496-x>
- de Castro LF, de Freitas SV, Duarte LC et al (2019) Salivary diagnostics on paper microfluidic devices and their use as wearable sensors for glucose monitoring. *Anal Bioanal Chem* 411:4919–4928. <https://doi.org/10.1007/s00216-019-01788-0>
- Dudala S, Dubey SK, Goel S (2019) Fully integrated, automated, and smartphone enabled point-of-source portable platform with microfluidic device for nitrite detection. *IEEE Trans Biomed Circuits Syst* 13:1518–1524. <https://doi.org/10.1109/TBCAS.2019.2939658>
- Ebrahimi Fana S, Paknejad M, Aminian M (2021) Paper based analytical devices for blood grouping: a comprehensive review. *Biomed Microdevices* 23:34. <https://doi.org/10.1007/s10544-021-00569-w>
- Eisenbrand G, Spiegelhalter B, Preussmann R (1980) Nitrate and Nitrite in Saliva *OCL* 37:227–231. <https://doi.org/10.1159/000225441>
- Elizalde E, Urteaga R, Berli CLA (2015) Rational design of capillary-driven flows for paper-based microfluidics. *Lab Chip* 15:2173–2180. <https://doi.org/10.1039/C4LC01487A>
- Ferreira FTSM, Mesquita RBR, Rangel AOSS (2020) Novel microfluidic paper-based analytical devices (μ PADs) for the determination of nitrate and nitrite in human saliva. *Talanta* 219:121183. <https://doi.org/10.1016/j.talanta.2020.121183>
- Ferreira FTSM, Catalão KA, Mesquita RBR, Rangel AOSS (2021) New microfluidic paper-based analytical device for iron determination in urine samples. *Anal Bioanal Chem* 413:7463–7472. <https://doi.org/10.1007/s00216-021-03706-9>
- Frenzel W, Schulz-Brüssel J, Zinvirt B (2004) Characterisation of a gas-diffusion membrane-based optical flow-through sensor exemplified by the determination of nitrite. *Talanta* 64:278–282. <https://doi.org/10.1016/j.talanta.2004.01.025>
- Gao H, Liu J-J, Liu Y-Q, Wu Z-Y (2019) Detection of urine protein by a paper-based analytical device enhanced with ion concentration polarization effect. *Microfluid Nanofluid*. <https://doi.org/10.1007/S10404-019-2220-3>
- Gidde RR, Pawar PM (2020) Flow feature and mixing performance analysis of RB-TSAR and EB-TSAR micromixers. *Microsyst Technol* 26:517–530. <https://doi.org/10.1007/s00542-019-04498-w>
- Govindaraj S, Daniel MJ, Vasudevan SS, Kumaran JV (2019) Changes in salivary flow rate, pH, and viscosity among working men and women. *Dentistry Med Res* 7:56. https://doi.org/10.4103/dmr.dmr_20_19
- Gravesen P, Branebjerg J, Jensen OS (1993) Microfluidics—a review. *J Micromech Microeng* 3:168–182. <https://doi.org/10.1088/0960-1317/3/4/002>
- Green LC, Wagner DA, Glogowski J et al (1982) Analysis of nitrate, nitrite, and [15N]nitrate in biological fluids. *Anal Biochem* 126:131–138. [https://doi.org/10.1016/0003-2697\(82\)90118-x](https://doi.org/10.1016/0003-2697(82)90118-x)
- Hao Z, Chen H, Shi X et al (2021) Fabrication for paper-based microfluidic analytical devices and saliva analysis application. *Microfluid Nanofluid* 25:80. <https://doi.org/10.1007/s10404-021-02476-1>
- He Q, Ma C, Hu X, Chen H (2013) Method for fabrication of paper-based microfluidic devices by alkylsilane self-assembling and UV/O₃-patterning. *Anal Chem* 85:1327–1331. <https://doi.org/10.1021/ac303138x>
- Hong SH, Shu J-I, Wang Y, Baysal O (2021) Automated optimization of double heater convective polymerase chain reaction devices based on CFD simulation database and artificial neural network model. *Biomed Microdevices* 23:20. <https://doi.org/10.1007/s10544-021-00551-6>
- Irandoost M, Shariati-Rad M, Haghghi M (2013) Nitrite determination in water samples based on a modified Griess reaction and central composite design. *Anal Methods* 5:5977–5982. <https://doi.org/10.1039/C3AY40913A>
- Jain M, Rao A, Nandakumar K (2013) Numerical study on shape optimization of groove micromixers. *Microfluid Nanofluid* 15:689–699. <https://doi.org/10.1007/s10404-013-1169-x>
- Jayawardane BM, Wei S, McKelvie ID, Kolev SD (2014) Microfluidic paper-based analytical device for the determination of nitrite and nitrate. *Anal Chem* 86:7274–7279. <https://doi.org/10.1021/ac5013249>
- Jobgen WS, Jobgen SC, Li H et al (2007) Analysis of nitrite and nitrate in biological samples using high-performance liquid chromatography. *J Chromatogr B Analyt Technol Biomed Life Sci* 851:71–82. <https://doi.org/10.1016/j.jchromb.2006.07.018>
- Kamali B, Asiaei S, Beigzadeh B, Ali Ebadi A (2018) Micro-lithography on paper, surface process modifications for biomedical performance enhancement. *Colloids Surf, A* 555:389–396. <https://doi.org/10.1016/j.colsurfa.2018.06.053>
- Karimi S, Mojaddam M, Majidi S et al (2021) Numerical and experimental analysis of a high-throughput blood plasma separator for point-of-care applications. *Anal Bioanal Chem* 413:2867–2878. <https://doi.org/10.1007/s00216-021-03190-1>
- Kishnani V, Park S, Nakate UT et al (2021) Nano-functionalized paper-based IoT enabled devices for point-of-care testing: a review. *Biomed Microdevices* 24:2. <https://doi.org/10.1007/s10544-021-00588-7>
- Klasner SA, Price AK, Hoeman KW et al (2010) Paper-based microfluidic devices for analysis of clinically relevant analytes present in urine and saliva. *Anal Bioanal Chem* 397:1821–1829. <https://doi.org/10.1007/s00216-010-3718-4>
- Koivunen R, Jutila E, Bollström R, Gane P (2016) Hydrophobic patterning of functional porous pigment coatings by inkjet printing. *Microfluid Nanofluid* 20:83. <https://doi.org/10.1007/s10404-016-1747-9>
- Kojić S, Birgermajer S, Radonić V et al (2020) Optimization of hybrid microfluidic chip fabrication methods for biomedical application. *Microfluid Nanofluid* 24:66. <https://doi.org/10.1007/s10404-020-02372-0>
- Li B, Fu L, Zhang W et al (2014) Portable paper-based device for quantitative colorimetric assays relying on light reflectance principle. *Electrophoresis* 35:1152–1159. <https://doi.org/10.1002/elps.201300583>
- Liu Y-C, Hsu C-H, Lu B-J et al (2018) Determination of nitrite ions in environment analysis with a paper-based microfluidic device. *Dalton Trans* 47:14799–14807. <https://doi.org/10.1039/C8DT02960A>
- Lopez-Ruiz N, Curto VF, Erenas MM et al (2014) Smartphone-based simultaneous pH and nitrite colorimetric determination for paper microfluidic devices. *Anal Chem* 86:9554–9562. <https://doi.org/10.1021/ac5019205>
- Lorente L, Gómez-Bernal F, Martín MM et al (2020) High serum nitrates levels in non-survivor COVID-19 patients. *Med Intensiva (Engl Ed)* S0210–5691(20):30336–30343. <https://doi.org/10.1016/j.medin.2020.10.003>
- Mai V-P, Ku C-H, Yang R-J (2019) Porosity estimation using electric current measurements for paper-based microfluidics. *Microfluid Nanofluid* 23:59. <https://doi.org/10.1007/s10404-019-2226-x>
- Martinez AW, Phillips ST, Butte MJ, Whitesides GM (2007) Patterned paper as a platform for inexpensive, low-volume, portable bioassays. *Angew Chem Int Ed Engl* 46:1318–1320. <https://doi.org/10.1002/anie.200603817>

- Mehrdel P, Karimi S, Farré-Lladós J, Casals-Terré J (2018) Novel variable radius spiral-shaped micromixer: from numerical analysis to experimental validation. *Micromachines* (Basel) 9:E552. <https://doi.org/10.3390/mi9110552>
- Miranda JM, Oliveira H, Teixeira JA et al (2010) Numerical study of micromixing combining alternate flow and obstacles. *Int Commun Heat Mass Transfer* 37:581–586. <https://doi.org/10.1016/j.icheatmasstransfer.2010.01.012>
- Moorcroft MJ, Davis J, Compton RG (2001) Detection and determination of nitrate and nitrite: a review. *Talanta* 54:785–803. [https://doi.org/10.1016/S0039-9140\(01\)00323-X](https://doi.org/10.1016/S0039-9140(01)00323-X)
- Nie J, Liang Y, Zhang Y et al (2012) One-step patterning of hollow microstructures in paper by laser cutting to create microfluidic analytical devices. *Analyst* 138:671–676. <https://doi.org/10.1039/C2AN36219H>
- Noiphung J, Nguyen MP, Punyadeera C et al (2018) Development of paper-based analytical devices for minimizing the viscosity effect in human saliva. *Theranostics* 8:3797–3807. <https://doi.org/10.7150/thno.24941>
- Osborn JL, Lutz B, Fu E et al (2010) Microfluidics without pumps: reinventing the T-sensor and H-filter in paper networks. *Lab Chip* 10:2659–2665. <https://doi.org/10.1039/C004821F>
- Patil Y, Dotseth K, Shapiro T et al (2020) Modular design of paper based switches for autonomous lab-on paper micro devices. *Biomed Microdevices* 23:1. <https://doi.org/10.1007/s10544-020-00537-w>
- Pattanayak P, Singh SK, Gulati M et al (2021) Microfluidic chips: recent advances, critical strategies in design, applications and future perspectives. *Microfluid Nanofluid* 25:99. <https://doi.org/10.1007/s10404-021-02502-2>
- Pignatelli P, Fabietti G, Ricci A et al (2020) How Periodontal Disease and Presence of Nitric Oxide Reducing Oral Bacteria Can Affect Blood Pressure. *Int J Mol Sci* 21:E7538. <https://doi.org/10.3390/ijms21207538>
- Reed PI, Haines K, Smith P et al (1981) Gastric juice N-nitrosamines in health and gastroduodenal disease. *Lancet*. [https://doi.org/10.1016/S0140-6736\(81\)90939-9](https://doi.org/10.1016/S0140-6736(81)90939-9)
- Rezk AR, Qi A, Friend JR et al (2012) Uniform mixing in paper-based microfluidic systems using surface acoustic waves. *Lab Chip* 12:773–779. <https://doi.org/10.1039/c2lc21065g>
- Rhouma R, Meherzi S, Belghith S (2009) OCML-based colour image encryption. *Chaos, Solitons Fractals* 40:309–318. <https://doi.org/10.1016/j.chaos.2007.07.083>
- Schaumburg F, Berli CLA (2019) Assessing the rapid flow in multilayer paper-based microfluidic devices. *Microfluid Nanofluid* 23:98. <https://doi.org/10.1007/s10404-019-2265-3>
- Schaumburg F, Urteaga R, Kler PA, Berli CLA (2018) Design keys for paper-based concentration gradient generators. *J Chromatogr A* 1561:83–91. <https://doi.org/10.1016/j.chroma.2018.05.040>
- Shariati S, Khayatian G (2022) A new method for selective determination of creatinine using smartphone-based digital image. *Microfluid Nanofluid* 26:30. <https://doi.org/10.1007/s10404-022-02538-y>
- Shinn MB (1941) Colorimetric Method for Determination of Nitrate. *Ind Eng Chem Anal Ed* 13:33–35. <https://doi.org/10.1021/i560089a010>
- Shrivastava A, Gupta V (2011) Methods for the determination of limit of detection and limit of quantitation of the analytical methods. *Chronicles of Young Scientists* 2:21–21
- Sukuroglu E, Güncü GN, Kilinc K, Caglayan F (2015) Using salivary nitrite and nitrate levels as a biomarker for drug-induced gingival overgrowth. *Front Cell Infect Microbiol* 5:87–95. <https://doi.org/10.3389/fcimb.2015.00087>
- Sun J, Zhang X, Broderick M, Fein H (2003) Measurement of nitric oxide production in biological systems by using Griess reaction assay. *Sensors* 3:276–284. <https://doi.org/10.3390/s30800276>
- Swain KK, Bhand S (2021) A colorimetric paper-based ATONP-ALP nanobiosensor for selective detection of Cd²⁺ ions in clams and mussels. *Anal Bioanal Chem* 413:1715–1727. <https://doi.org/10.1007/s00216-020-03140-3>
- Tesfaye T, Hussen A (2022) Microfluidic paper-based analytical device (μPAD) fabricated by wax screen printing technique for the determination of nitrite and nitrate ion in water samples. *Microfluid Nanofluid* 26:22. <https://doi.org/10.1007/s10404-022-02520-8>
- Trofimchuk E, Hu Y, Nilghaz A et al (2020) Development of paper-based microfluidic device for the determination of nitrite in meat. *Food Chem* 316:126396. <https://doi.org/10.1016/j.foodchem.2020.126396>
- Tseng C-C, Kung C-T, Chen R-F et al (2021) Recent advances in microfluidic paper-based assay devices for diagnosis of human diseases using saliva, tears and sweat samples. *Sens Actuators, B Chem* 342:130078. <https://doi.org/10.1016/j.snb.2021.130078>
- Tsikis D (2007) Analysis of nitrite and nitrate in biological fluids by assays based on the Griess reaction: appraisal of the Griess reaction in the L-arginine/nitric oxide area of research. *J Chromatogr B Analyt Technol Biomed Life Sci* 851:51–70. <https://doi.org/10.1016/j.jchromb.2006.07.054>
- Urteaga R, Elizalde E, Berli CLA (2018) Transverse solute dispersion in microfluidic paper-based analytical devices (μPADs). *Analyst* 143:2259–2266. <https://doi.org/10.1039/C8AN00149A>
- Verma N, Patel D, Pandya A (2020) Emerging diagnostic tools for detection of COVID-19 and perspective. *Biomed Microdevices* 22:83. <https://doi.org/10.1007/s10544-020-00534-z>
- Wang P, Wang M, Zhou F et al (2017) Development of a paper-based, inexpensive, and disposable electrochemical sensing platform for nitrite detection. *Electrochem Commun* 81:74–78. <https://doi.org/10.1016/j.elecom.2017.06.006>
- Wang H, Wan N, Ma L et al (2018) A novel and simple spectrophotometric method for detection of nitrite in water. *Analyst* 143:4555–4558. <https://doi.org/10.1039/C8AN01063C>
- Wang K, Yang J, Xu H et al (2020) Smartphone-imaged multilayered paper-based analytical device for colorimetric analysis of carcinoembryonic antigen. *Anal Bioanal Chem* 412:2517–2528. <https://doi.org/10.1007/s00216-020-02475-1>
- Wang J, Mei F, Bai L et al (2021a) Serum nitrite and nitrate: A potential biomarker for post-covid-19 complications? *Free Radic Biol Med* 175:216–225. <https://doi.org/10.1016/j.freeradbiomed.2021.08.237>
- Wang M, Song Z, Jiang Y et al (2021b) A three-dimensional pinwheel-shaped paper-based microfluidic analytical device for fluorescence detection of multiple heavy metals in coastal waters by rational device design. *Anal Bioanal Chem* 413:3299–3313. <https://doi.org/10.1007/s00216-021-03269-9>
- Yetisen AK, Akram MS, Lowe CR (2013) Paper-based microfluidic point-of-care diagnostic devices. *Lab Chip* 13:2210–2251. <https://doi.org/10.1039/C3LC50169H>
- Yıldırım G, Akgöl S, Arica Y et al (2003) Polyhydroxyethylmethacrylate/polyhydroxybutyrate composite membranes for fluoride release. *J Appl Polym Sci* 87:976–981. <https://doi.org/10.1002/app.11397>
- Zaglavara F, Jimack PK, Kapur N et al (2022) Multi-objective optimisation of polymerase chain reaction continuous flow systems. *Biomed Microdevices* 24:16. <https://doi.org/10.1007/s10544-022-00610-6>

- Zhang K, Ren Y, Hou L et al (2018a) An efficient micromixer actuated by induced-charge electroosmosis using asymmetrical floating electrodes. *Microfluid Nanofluid* 22:130. <https://doi.org/10.1007/s10404-018-2153-2>
- Zhang X-X, Song Y-Z, Fang F, Wu Z-Y (2018b) Sensitive paper-based analytical device for fast colorimetric detection of nitrite with smartphone. *Anal Bioanal Chem* 410:2665–2669. <https://doi.org/10.1007/s00216-018-0965-2>

Publisher's Note Springer Nature remains neutral with regard to jurisdictional claims in published maps and institutional affiliations.

Springer Nature or its licensor holds exclusive rights to this article under a publishing agreement with the author(s) or other rightsholder(s); author self-archiving of the accepted manuscript version of this article is solely governed by the terms of such publishing agreement and applicable law.